IET Microwaves, Antennas & Propagation

*Special Issue: Selected Papers from the 11th European Conference on Antennas and Propagation (EuCAP 2017)*

# Characterising THz propagation and intrabody thermal absorption in iWNSNs

ISSN 1751-8725
Received on 26th June 2017
Revised 5th January 2018
Accepted on 14th January 2018
E-First on 19th February 2018
doi: 10.1049/iet-map.2017.0603
www.ietdl.org

*Hadeel Elayan[1], Raed M. Shubair[2] ✉, Josep M. Jornet[3]*

[1]*Department of Electrical and Computer Engineering, Khalifa University, UAE*
[2]*Research Laboratory of Electronics, Massachusetts Institute of Technology, USA*
[3]*Department of Electrical Engineering, University at Buffalo, The State University of New York, USA*
✉ *E-mail: rshubair@mit.edu*

**Abstract:** Nanosized devices operating inside the human body will eventually facilitate transformative health monitoring and diagnosis systems. The interconnection of these implantable nanosensors forms an in vivo wireless nanosensor network (iWNSN), which allows autonomous data transmission and enables sensing, coordination, and control among its entities. In specific, with the development of miniature plasmonic signal sources, antennas and detectors, wireless communications among nanodevices points towards the terahertz band (0.1–10 THz) as a suitable platform and feasible wireless range to initiate intrabody communication. In this study, a rigorous channel model for intrabody communication in iWNSNs is developed. The total path loss is computed by taking into account the contribution of the spreading of the propagating wave, molecular absorption from human tissues, as well as scattering from both small and large body particles. The presented model is further complemented by investigating the photo-thermal interactions which arise from absorption at the THz frequency band. The aforementioned study which analyzes the propagation of electromagnetic signals inside the human body is fundamental to assess the feasibility of the THz frequency band, determine the requirements and controlling parameters of a THz intrabody system as well as highlight the health issues correlated with operating at such frequencies.

## 1 Introduction

The engineering community is witnessing a new frontier in the communication industry. Among others, the tools provided by nanotechnologies enable the development of novel nanosensors and nanomachines. On the one hand, nanosensors are capable of detecting events with unprecedented accuracy. On the other hand, nanomachines are envisioned to accomplish tasks ranging from computing and data storing to sensing and actuation [1]. Recently, in vivo nanosensing systems have been presented to provide fast and accurate disease diagnosis and treatment. These systems will be capable of operating inside the human body in real time and will be of great benefit for medical monitoring and medical implant communication [2].

Despite the fact that nanodevice technology has been witnessing great advancements, enabling the communication among nanomachines is still a major challenge. Classical communication paradigms need to undergo a profound revision before being used in nanonetworks. One of the mechanisms being comprehensively investigated is molecular communication [3], which is based on the exchange of molecules to transmit information. However, there are still many fundamental challenges to address, including the development of methods to overcome the very long latency in molecular systems or the potential interference with biological molecular processes. Ultrasonic communication, based on the use of very high frequency acoustic signals, has also been recently introduced [4]. Nonetheless, for the time being, the size and power limitations of ultrasonic acoustic transducers pose a major challenge in their integration with biological nanosensors.

From the electromagnetic perspective, the miniaturisation of a conventional metallic antenna to meet the size requirements of a nanosensor results in very high resonant frequencies, in the order of several hundreds of terahertz (THz or $10^{12}$ Hz). Accordingly, novel plasmonics has been recently proposed for wireless communication among nanodevices [5]. These nanoantennas enable the wireless interconnection amongst nanosensors deployed inside and over the human body resulting in many nano-biosensing applications [6]. For the time being, several works exist pointing to both the terahertz band (0.1–10 THz) as well as the infrared and optical transmission windows [7, 8]. While the majority of nano-biosensing applications rely on the use of light, the propagation of THz signals within the human body remains largely unknown.

In this study, a novel channel model for intrabody communication in the THz band is presented. In particular, a mathematical framework is developed to compute the path loss by taking into account the spreading of the propagating wave, absorption from different types of molecules, as well as scattering of both the cells and the medium background. The proposed framework verifies the feasibility of using the THz band to establish in vivo wireless nanosensor networks (iWNSNs). An earlier version of this work is available in [9]. In addition, for the completeness of the work, the effect of molecular absorption is further assessed. In specific, the impact of molecular vibration due to the absorption is captured by analysing the heat generation and temperature increase experienced by cells exposed to THz electromagnetic radiation. This photo-thermal effect at THz frequencies is controlled by certain parameters including the THz signal duration and strength. Thereby, the results attained will have benefits from both the communication as well as biomedical perspectives in which efficient intrabody communication strategies could be developed and various in-vivo applications could be enabled. The rest of the paper is organised as follows. In Section 2, we discuss intrabody wave propagation losses considering the effect of spreading, molecular absorption as well as scattering. In Section 3, absorption is analysed by evaluating the temperature increase witnessed as a result of the intrabody particles' vibration. In Section 4, the numerical results of the mathematical models are illustrated and validated via electromagnetic wave propagation simulation. Finally, we draw our conclusions in Section 5.

## 2 Characterising THz intrabody propagation

The total path loss in the THz band is contributed by three frequency-dependent terms: the spreading loss factor $L_{spr}(f)$, the molecular absorption loss factor $L_{abs}(f)$ and the scattering loss factor $L_{sca}(f)$. Each of these terms represents the ratio of the output

to input powers for a particular intrabody distance. More specifically, the total attenuation factor is given by

$$L_{\text{tot}}(f) = L_{\text{spr}}(f) \cdot L_{\text{abs}}(f) \cdot L_{\text{sca}}(f). \quad (1)$$

The analytical model which will be presented in this study focuses on the frequencies between 0.1 and 10 THz or, equivalently, wavelengths between 30 μm and 3 mm. Moreover, since the THz band lies in the middle ground between microwaves/millimeter waves and infrared, both frequency ($f$) and wavelength ($\lambda$) are common notations.

### 2.1 Intrabody path loss due to wave spreading in human tissue

Electromagnetic waves suffer from the spreading of energy, which is quantitatively described in the case of spherical propagation by the well-known inverse-squared distance function

$$L_{\text{spr}} = D\left(\frac{\lambda_{\text{g}}}{4\pi d}\right)^2, \quad (2)$$

where $\lambda_{\text{g}}$ is the effective wavelength, $\lambda/n'$, $n'$ and $n''$ are the real and imaginary parts of the tissue refractive index $n$, respectively. The tissue refractive index $n$ is given by

$$n = n' - \text{j}n''. \quad (3)$$

It is worth noting that $n = \sqrt{\epsilon_{\text{r}}}$, where $\epsilon_{\text{r}}$ is the relative permittivity. The relative permeability is accounted for $\mu_{\text{r}} = 1$ since the biological tissues show almost no magnetic behaviour [10].

The directivity, $D$, refers to the maximum gain of the nanoantenna and is given by the ratio of the maximum power density $P(\theta, \phi)_{\max}$ in (W/m$^2$) to its average value over a sphere, as observed in the far field of an antenna. Thus

$$D = \frac{P(\theta, \phi)_{\max}}{P(\theta, \phi)_{\text{av}}}. \quad (4)$$

From [11], the final form of the directivity is given by

$$D = \frac{4\pi}{\int\int_{4\pi} P_{\text{n}}(\theta, \phi)\text{d}\Omega} = \frac{4\pi}{\Omega_{\text{A}}}, \quad (5)$$

where $P_{\text{n}}(\theta, \phi)\text{d}\Omega = P(\theta, \phi)/P(\theta, \phi)_{\max}$ is the normalised power pattern, and $\Omega_{\text{A}}$ refers to the radiation solid angle. This angle depends on the specific radiation diagram of the source and antenna being used. For example, for a directional source with a narrow beam of width $\Delta\theta$, $\Omega_{\text{A}}$ is given as

$$\Omega_{\text{A}} = \int_{\phi=0}^{2\pi}\int_{\theta=0}^{\Delta\theta} \sin\theta \text{d}\theta\text{d}\phi = 2\pi(1 - \cos\Delta\theta). \quad (6)$$

A more realistic approach which mimics a THz source would be to consider a light source with a Gaussian beam which has a radiation pattern given by [12]

$$E_\theta = \frac{1}{2}(1 + \cos\theta). \quad (7)$$

Since the radiated power, $P$, is proportional to $E_\theta^2$, the solid angle, $\Omega_{\text{A}}$ of a Gaussian beam of width $\Delta\theta$ is given as

$$\begin{aligned}\Omega_{\text{A}} &= \int_{\phi=0}^{2\pi}\int_{\theta=0}^{\Delta\theta} \frac{1}{4}(1 + 2\cos\theta + \cos^2\theta)\sin\theta \text{d}\theta\text{d}\phi \\ &= \frac{\pi}{2}\left[\frac{8}{3} - (\cos\Delta\theta + \cos^2\Delta\theta + \frac{1}{3}\cos^3\Delta\theta)\right].\end{aligned} \quad (8)$$

### 2.2 Intrabody path loss due to molecular absorption by human tissue

Molecules present in a standard medium are excited by electromagnetic waves at specific frequencies within the THz band. An excited molecule internally vibrates, in which the atoms show periodic motion, while the molecule as a whole has constant translational and rotational motions. It must be noted that the THz waves are non-ionising in which they induce vibration, but cannot break molecules. Due to this vibration, part of the energy of the propagating wave is converted into kinetic energy or, from the communication perspective, simply lost. Hence, molecular absorption is calculated by computing the fraction of the incident electromagnetic radiation that is able to pass through the medium at a given frequency. Using the Beer–Lambert law [13], attenuation due to molecular absorption for an electromagnetic travelling wave at a distance, $d$, is given by

$$L_{\text{abs}} = \text{e}^{-\mu_{\text{abs}}d}, \quad (9)$$

where $\mu_{\text{abs}}$ is the molecular absorption coefficient. This coefficient depends on the composition of the medium and was first introduced and computed for gas molecules by Jornet *et al.* in [14]. In the context of intrabody communications, the same approach is followed since the body is composed of nanoscale biomolecular structures. These include chromophores, which are compounds in our tissues responsible for absorbing light radiation. Each molecule has a spectrum of absorption that can quickly change even for small wavelength variations. The disruption of the medium optical uniformity can be expressed in the non-uniformity of the refractive index throughout the medium [15]. Hence, the molecular absorption coefficient can be calculated using

$$\mu_{\text{abs}} = \frac{4\pi n''}{\lambda_{\text{g}}}. \quad (10)$$

To estimate the absorption coefficient, we can follow two different strategies. On the one hand, we can model the absorption from individual particles. The efficiency of a particle to absorb radiation can be expressed by the absorption efficiency

$$\eta_{\text{abs}} = \frac{\sigma_{\text{abs}}}{\sigma_{\text{g}}}, \quad (11)$$

where $\sigma_{\text{abs}}$ is the molecular absorption cross section and $\sigma_{\text{g}} = \pi r^2$ is the geometric cross section. The absorption coefficient, $\mu_{\text{abs}}$, can be then obtained as

$$\mu_{\text{abs}} = \frac{N_0}{V_0}\eta_{\text{abs}}\sigma_{\text{g}}, \quad (12)$$

where $N_0$ is the number of particles in volume $V_0$. At this stage, the main challenge is to estimate the value of $\eta_{\text{abs}}$. This is a rather complex task, especially when different types of molecules with different frequency responses are considered. It is to be noted that such a relation holds in the particular situation of spherically-shaped particles having the same radius, $r$.

On the other hand, provided that we are dealing with a large number of molecules, it is common to consider the effective medium assumption. In specific, the dielectric response in the frequency domain of tissues having high water content can be characterised by the Debye relaxation model [16], which describes the reorientation of molecules that could involve translational and rotational diffusion, hydrogen bond arrangement, and structural rearrangement. For a pure material, multiple Debye processes are possible where the complex permittivity is described by [17]

$$\epsilon(\omega) = \epsilon_\infty + \sum_{j=1}^{n} \frac{\Delta\epsilon}{1 + \text{j}w\tau_j}, \quad (13)$$

**Table 1** Permittivity and relaxation time values

| Model | $\epsilon_\infty$ | $\epsilon_1$ | $\epsilon_2$ | $\tau_1$, ps | $\tau_2$, ps |
|---|---|---|---|---|---|
| water [19] | 3.3 | 78.8 | 4.5 | 8.4 | 0.1 |
| whole blood [19] | 2.1 | 130 | 3.8 | 14.4 | 0.1 |
| skin [16] | 3.0 | 60.0 | 3.6 | 10.0 | 0.2 |

in which $\epsilon_\infty$ is the permittivity at the high frequency limit, $\Delta\epsilon = \epsilon_j - \epsilon_{j+1}$, $\epsilon_j$ are intermediate values, occurring at different times of the permittivity, $\tau_j$ is the relaxation time relating to the $j$th Debye type relaxation process, and $\omega$ is the angular frequency given as $2\pi f$.

Biological tissues are principally an assembly of biological cells, each with different sub-cellular components that exhibit different responses and relaxation times. To provide the best approximation of complex permittivity for polar liquids at frequencies up to 1 THz, the double Debye equations are used [18]

$$\epsilon(\omega) = \epsilon_\infty + \frac{\epsilon_1 - \epsilon_2}{1 + \mathrm{j}\omega\tau_1} + \frac{\epsilon_2 - \epsilon_\infty}{1 + \mathrm{j}\omega\tau_2}. \tag{14}$$

Equation (14) is rationalised and the real and imaginary parts of the complex permittivity are separated as follows:

$$\epsilon'(\omega) = \epsilon_\infty + \frac{\epsilon_1 - \epsilon_2}{1 + (\omega\tau_1)^2} + \frac{\epsilon_2 - \epsilon_\infty}{1 + (\omega\tau_2)^2}, \tag{15}$$

$$\epsilon''(\omega) = \frac{(\epsilon_1 - \epsilon_2)(\omega\tau_1)}{1 + (\omega\tau_1)^2} + \frac{(\epsilon_2 - \epsilon_\infty)(\omega\tau_2)}{1 + (\omega\tau_2)^2}. \tag{16}$$

Using the values in Table 1, $\epsilon'(\omega)$ and $\epsilon''(\omega)$ are computed. These values are then used to calculate (10) by using the relation in (3) and knowing that $\epsilon_r(\omega) = \epsilon'(\omega) - \mathrm{j}\epsilon''(\omega)$. Thereby, the attenuation due to molecular absorption, $L_{abs}$, given in (9) is computed at the THz band.

### 2.3 Intrabody path loss due to scattering by human tissue

From the nanosensor perspective, the body is a collection of different types of composites, such as cells, organelles, proteins, and molecules with different geometry and arrangement as well as different electromagnetic properties. Scattering by particles affects the propagation of the electromagnetic wave due to the deflection of the beam caused by the microscopic non-uniformities present in the human body. This propagation phenomenon depends on the size, shape, and refractive index of the individual particle as well as on the wavelength of the incident beam [20]. Rayleigh and Mie theories describe the scattering processes on small spherical objects. When the scattering particle diameters are smaller than the wavelength of the propagating electromagnetic wave, Rayleigh scattering occurs. However, when the particle diameters are approximately equal to the wavelength of the electromagnetic wave, Mie scattering takes place [21]. When the objects are large compared with wavelength, specular, or geometric scattering occurs [22].

The most important characteristic of a scattered wave is its intensity, $I_{sca}$, expressed as [23]

$$I_{sca} r^2 \sin\theta \mathrm{d}\theta \mathrm{d}\phi = \frac{1}{k^2} I_{inc} S(\theta, \phi) \sin\theta \mathrm{d}\theta \mathrm{d}\phi, \tag{17}$$

or

$$I_{sca} = \frac{1}{(kr)^2} I_{inc} S(\theta, \phi), \tag{18}$$

where $k = 2\pi/\lambda$ is the wave number of the incident radiation, $I_{inc}$ is the incident intensity, and $S(\theta, \phi)$ is the scattering amplitude function. In addition to the intensity function, the scattering cross section and the scattering efficiency are needed to characterise the scattering loss. To derive the scattering cross section, $\sigma_{sca}$, let the total energy scattered in all directions by the particle be equal to the incident beam falling on the area as follows [23]:

$$\begin{aligned} \sigma_{sca} &= \frac{1}{I_{inc}} \int_0^{2\pi} \int_0^{\pi} I_{sca} r^2 \sin\theta \mathrm{d}\theta \mathrm{d}\phi \\ &= \frac{1}{(k)^2} \int_0^{2\pi} \int_0^{\pi} S(\theta, \phi) \sin\theta \mathrm{d}\theta \mathrm{d}\phi, \end{aligned} \tag{19}$$

where the scattering amplitude function, $S(\theta, \phi)$ of a sphere that mimics a particle is given by

$$S(\theta, \phi) = \frac{k^2}{4\pi} \int_{\mathfrak{A}} \mathrm{e}^{-\mathrm{i}k\xi\sin\theta(\xi\cos\phi + \eta\sin\phi)} (1 + \cos\theta) \mathrm{d}\xi \mathrm{d}\eta, \tag{20}$$

in which $\mathfrak{A}$ is the planar aperture. Since both a sphere and an opaque disk have the same diffraction pattern, the scattering amplitude of a disk is considered for simplicity as it is independent of the azimuthal angle $\phi$

$$S(\theta) = \frac{k^2}{4\pi} \int_{\mathfrak{A}} \mathrm{e}^{-\mathrm{i}k\xi\sin\theta} (1 + \cos\theta) \mathrm{d}\xi. \tag{21}$$

The integral evaluation is present in [24].

Analogous to absorption, the scattering efficiency, $\eta_{sca}$, represents the ratio of the energy scattered by the particle to the total energy in the incident beam intercepted by the geometric cross section of the particle and is given by

$$\eta_{sca} = \frac{\sigma_{sca}}{\sigma_g}. \tag{22}$$

These values depend largely on the size of the particles. In our model, we consider the scattering from both small molecules as well as relatively large cells. The signal attenuation attributes to scattering is represented by an exponential decay factor that involves the scattering coefficient, as will be explained in the subsequent sections.

*2.3.1 Scattering by particles:* For particles much smaller than the wavelength, the local electric field produced by the wave is approximately uniform at any instant. This applied electric field induces a dipole in the particle. Since the electric field oscillates, the induced dipole oscillates; and according to classical theory, the dipole radiates in all directions. This type of scattering is called *Rayleigh scattering* [25].

The scattering efficiency of small spherical absorbing particles is given by [26]

$$\eta_{sca}^{small} = \frac{8}{3} \psi^4 \mathrm{Re}\left(\frac{n^2 - 1}{n^2 + 2}\right)^2, \tag{23}$$

where $\psi = 2\pi r/\lambda_g$ is the dimensionless size parameter of the particle. Following a similar approach as before, we can now obtain the scattering coefficient for small particles as

$$\mu_{sca}^{small} = \rho_v \eta_{sca}^{small} \sigma_g. \tag{24}$$

*2.3.2 Scattering by cells:* Scattering by large particles can be studied by applying van de Hulst approximation, which is also referred to as the anomalous diffraction approximation [26]. Indeed, the total energy removed from the incident beam, the

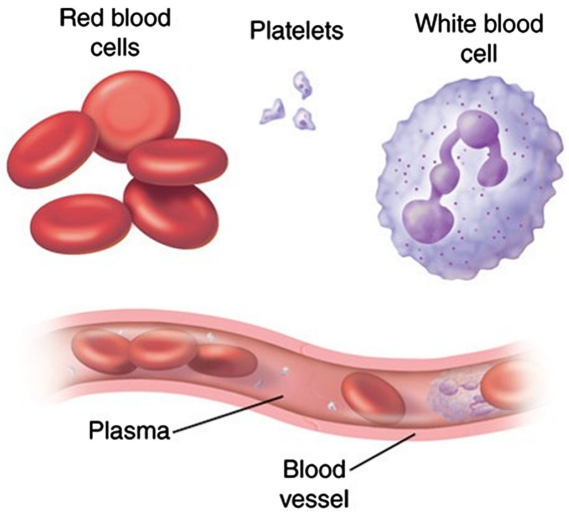


**Fig. 1** *Blood components*

extinction energy, is the sum of the energy scattered and absorbed. The corresponding extinction efficiency is given by [27]

$$\eta_{\text{ext}} = 2 - \frac{4}{p}\sin p + \frac{4}{p^2}(1 - \cos p), \tag{25}$$

in which

$$\eta_{\text{sca}}^{\text{large}} = \eta_{\text{ext}} - \eta_{\text{abs}}, \tag{26}$$

where $p = 4\pi r(n-1)/\lambda_{\text{g}} = 2(n-1)\psi$ represents the phase delay of the wave passing through the centre of the particle. The complete derivation of (25) can be found in [27]. A good example where scattering from various components can be illustrated is within the human blood. As conceptually depicted in Fig. 1, the blood is composed of various components. Blood plasma is the liquid component of the blood and is a mixture of mostly water (up to 95% by volume) and tiny particles of dissolved protein, glucose, minerals, and so forth. It also holds different types of blood cells in suspension, which are considered as the larger particles of the blood, namely, platelets (2 μm in diameter), red blood cells (7 μm), and white blood cell (up to 20 μm).

Combining (26) and (25) in (24), we can now obtain the scattering by large particles as

$$\mu_{\text{sca}}^{\text{large}} = \rho_{\text{v}}\eta_{\text{sca}}^{\text{large}}\sigma_{\text{g}}. \tag{27}$$

Finally, attenuation due to scattering is obtained from the addition of the scattering coefficient for both large and small particles and is given as

$$L_{\text{sca}} = \text{e}^{-\left(\mu_{\text{sca}}^{\text{small}} + \mu_{\text{sca}}^{\text{large}}\right)d}, \tag{28}$$

where $d$ is the propagation distance.

## 3 Characterising intrabody THz thermal absorption

Molecular absorption, presented in Section 2.2, is a phenomenon that not only compromises the propagation of electromagnetic signals in the body but results in a photo-thermal effect which ought to be assessed to analyse its impact on the design of communication strategies suited to the THz intrabody paradigm. In particular, due to the electromagnetic radiation of nanoantennas, the human body particles will seize part of the electromagnetic energy. Consequently, the absorbed power will activate the vibration of the particles resulting in heat generation and temperature increase. This thermal effect could then be converted into noise by defining the transmission bandwidth. It is to be noted that in the context of intrabody communication, few works exist in the literature [28, 29] that investigate molecular absorption noise; however, this is the first work which provides insight into the diffusive heat flow perspective of the intrabody noise.

Our system of interest is composed of a medium full of both biological cells as well as liquid-surrounded heat sources larger than tens of nm. The heat sources in this work are considered to be nanoantennas in nano-biosensing implants in the human body. As these nanoantennas radiate electromagnetic waves, cells will capture part of this energy through the process of molecular absorption. Hence, subsequent to such an exposure, the cells also become heat sources. The absorbed electromagnetic energy will then be converted into heat which will result in temperature increase around the cells. Therefore, the objective of our study is to compute the total temperature increase in the medium.

When considering the heat generation from an assembly of particles in close proximity, the temperature increase, $\Delta T_{\text{tot}}$, will stem from both self-contribution, $\Delta T_{\text{s}}$, as well as external contributions, $\Delta T_{\text{ext}}$. As a result, $\Delta T_{\text{tot}}$, which represents the total temperature increase experienced by the system is given as

$$\Delta T_{\text{tot}} = \Delta T_{\text{s}} + \Delta T_{\text{ext}}. \tag{29}$$

On the one hand, the maximum temperature increase due to a single particle, $\Delta T_{\text{s}}$, is given as

$$\Delta T_{\text{s}} = \frac{Q}{4\pi\kappa_0 r}, \tag{30}$$

where $Q$ is the total amount of heat production and $\kappa_0$ is the thermal conductivity of the medium. By the conservation of energy, the total amount of heat production $Q$ is divided into, $Q_{\text{in}}$, which represents the heat generated by the particle and, $Q_{\text{out}}$, which represents the heat dissipated by the particle. $Q_{\text{in}}$ is given by [30]

$$Q_{\text{in}} = \mu_{\text{abs}} I_0 V_{\text{p}}, \tag{31}$$

where $\mu_{\text{abs}}$ is the particle absorption coefficient which has been computed in (12), $V_{\text{p}}$ is the particle volume, and $I_0$ is the light intensity. At this stage, the relation between the generated heat and the molecular absorption path loss could be stemmed following the relations in (9) and (12). $Q_{\text{out}}$ is represented as

$$Q_{\text{out}} = -4\pi r^2 \kappa_{\text{eff}} \frac{\text{d}T}{\text{d}r} = 4\pi r \kappa_{\text{eff}} \Delta T, \tag{32}$$

in which $\kappa_{\text{eff}} = (\kappa_{\text{p}} + \kappa_0/2)$ is the effective thermal conductivity which is the average of both the particle and medium thermal conductivities, respectively. According to the law of conservation of energy, the amount of heat generated is equivalent to the amount of heat dissipated. As a result, the change in temperature of the surface of a particle experiences can be found by equating $Q_{\text{in}}$ and $Q_{\text{out}}$ as follows:

$$\Delta T = \frac{\mu_{\text{abs}} I_0 V_{\text{p}}}{4\pi r \kappa_{\text{eff}}}. \tag{33}$$

On the other hand, $\Delta T_{\text{ext}}$ results from the heat delivered by the other $N_{\text{p}} - 1$ particles located at $\boldsymbol{r_m}$ from a reference particle $\boldsymbol{r_n}$, and can be expressed as [31]

$$\Delta T_{\text{ext}} = \sum_{\substack{m=0 \\ m \neq n}}^{N_{\text{p}}} \frac{Q_m}{4\pi\kappa_{\text{eff}}} \frac{1}{|\boldsymbol{r_n} - \boldsymbol{r_m}|}, \tag{34}$$

where the coefficient, $Q_m$, describes the heat produced by the $N_{\text{p}}$ particles and each particle is treated as a point-like source of heat. To develop an expression to the collective temperature increase, $\Delta T_{\text{ext}}$, we follow an approach similar to the one in [32]. To carry out the derivation, an array of identical particles ($Q_m = Q_0$) extending over a circular area of diameter, $D$, is considered. The

unit cell area is, $A$, which depends on the particle inter-distance. Fig. 2 represents the aforementioned system.

The differential heat power delivered by an elementary area d$x$d$y$, located at the position $(x, y)$, is

$$\mathrm{d}^2Q(x,y) = Q_0\frac{\mathrm{d}x\mathrm{d}y}{A}. \tag{35}$$

This delivered power contributes to a temperature increase at the centre of the array as

$$\mathrm{d}^2T(x,y) = \frac{\mathrm{d}^2Q(x,y)}{4\pi\kappa_{\mathrm{eff}}\sqrt{x^2+y^2}}, \tag{36}$$

$$\mathrm{d}^2T(x,y) = \frac{Q_0\mathrm{d}x\mathrm{d}y}{4\pi\kappa_{\mathrm{eff}}A\sqrt{x^2+y^2}}. \tag{37}$$

By noticing that $\mathrm{d}x\mathrm{d}y = \sqrt{x^2+y^2}\mathrm{d}r\mathrm{d}\theta$, the total temperature increase is given by

$$\Delta T_{\mathrm{ext}} = \int_0^{2\pi}\int_0^{D/2}\frac{Q_0}{4\pi\kappa_{\mathrm{eff}}A}\mathrm{d}r\mathrm{d}\theta. \tag{38}$$

It must be noted that $\Delta T_{\mathrm{ext}}$ excludes the contribution of the source itself. Therefore, the limits must be interchanged where the integral will run over the distance from $\sqrt{A/\pi}$ instead of 0 in order to omit the contribution of the source area, which yields

$$\Delta T_{\mathrm{ext}} = \frac{Q_0}{2\pi\kappa_{\mathrm{eff}}\sqrt{(A/\pi)}}\left(1-\frac{2\sqrt{A}}{\sqrt{\pi}D}\right). \tag{39}$$

Furthermore, various expressions of $\Delta T_{\mathrm{ext}}$ exist depending on the typical array geometry and various illumination conditions. In general, these formulae follow Govoro's general trend found in [32] which provide an estimate to the total temperature increase under various system structures.

## 4 Numerical results

In this section, we first numerically evaluate the analytical models for spreading, absorption and scattering presented in Section 2, by taking into account realistic parameters of the intrabody properties (summarised in Table 1). We then calculate the total path loss and validate the results via electromagnetic wave simulations. Later, we investigate the mathematical formulation given in Section 3 in order to compute the total temperature increase experienced by the multiple particles available in the human body and assess its effect on THz intrabody communication systems.

### 4.1 Absorption

Fig. 3 illustrates the variation of the molecular absorption coefficient, $\mu_{\mathrm{abs}}$, provided in (10) along with the Debye model relations provided in Section 2.2 for different human tissues at the THz frequency band. It is evident from Fig. 3 that the effect of molecular absorption is more dominant in blood compared with other types of human tissues, which is expected since blood plasma is the liquid component of blood contributing to 55% of the body total blood volume [33]. It must be noted that the reason behind the high absorption in the THz band is the fact that the rotation transition of water molecules is located in this band.

### 4.2 Scattering

As for the effect of scattering, (24) and (27) can be used taking into consideration the radii of the various body particles as given in Table 2. It should be noted that the size of the scatterers at THz is much smaller than the wavelength of the propagating THz wave. Results of the scattering coefficient, $\mu_{\mathrm{sca}}$, given in Fig. 4 is almost negligible compared with its counterpart, absorption, shown in Fig. 3. This finding makes sense because the scattering effect is only significant for wavelengths that are much smaller than scatterer dimensions, unlike the current case in which we are investigating scattering at the THz wavelengths. This adds to the advantages of incorporating the THz band for intrabody communication because the propagating signal will not suffer from the scattering effects which are more significant in the higher optical frequencies. Based on the above finding, only the spreading and absorption losses contribute to the total path loss at the THz frequency band (Fig. 4).

### 4.3 Path loss

In this subsection, the theoretical model presented in Section 2 and used to calculate the total path loss experienced due to intrabody wave propagation presented in (1) is validated using COMSOL Multiphysics. A homogeneous medium with the same parameters that are used for the theoretical model has been taken to account by considering a circular cross section composed of the three main layers of human tissues, namely, skin, blood, and water. A point dipole antenna is chosen as the electromagnetic wave radiation source and the wave propagation has been simulated for up to 10 mm far from the antenna for the THz frequencies. The radiated power by a dipole antenna can be written as

$$P_{\mathrm{rad}} = (\pi\eta/3)|I_0 l/\lambda|^2, \tag{40}$$

where $I_0$ is the input current, $l$ is the antenna length and the product $I_0 l = 1$. The whole medium is enclosed by a perfect matched layer (PML). The PML is utilised to mimic the infinite environment and its thickness is half wavelength. The graphical representation of the model is demonstrated in Fig. 5.

The total path loss between two nanodevices operating at the THz frequency given in (1) is presented in Fig. 6 for a short range communication scenario. It can be seen that the developed model agrees with the finite-element method simulation which proves that the model is accurate enough. It must be highlighted that due to the recent advancements in THz technologies, novel THz transmitters and receivers have been developed facilitating the communication between nanodevices and opening the door to potentially biocompatible applications of iWNSNs.

### 4.4 Link budget analysis

In any communication system design, link budget analysis is the essential starting point for estimating the different losses encountered as the signal propagates from the transmitter to the receiver. A comprehensive and accurate model that predicts all the losses within the communication link is important for predicting the required transmitter power as well as the required receiver sensitivity. In radiofrequency system design, link budget estimations have been studied extensively, ranging from several hundred MHz for radiofrequency identifications [35, 36] to several THz for broadband wireless [37].

In the context of intrabody communication, the literature lacks link budget analysis between nanodevices operating within the human body. To perform such calculation, the gains and losses from the transmitter, through the medium (in this case the human body) to the receiver in a telecommunication system must be taken into account. The link budget equation is given as

$$P_{\mathrm{R}}(\mathrm{dB}) = P_{\mathrm{T}} + G_{\mathrm{T}} - \mathrm{Losses} + G_{\mathrm{R}}, \tag{41}$$

where $P_{\mathrm{R}}$ and $P_{\mathrm{T}}$ are the received and transmitted powers, respectively. $G_{\mathrm{T}}$ and $G_{\mathrm{R}}$ are the gains of the transmitting and receiving antennas, respectively.

Knowing the relationship between the signal to noise ratio (SNR), the received power, $P_{\mathrm{R}}$(dB), and the minimum receiver sensitivity, a system designer can infer the capability of THz detectors to capture the intrabody propagating signal. Using the parameters in Table 3, it can be deduced that a minimum receiver sensitivity value of −105.8 dBW (26.3 pW) is required. Based on the available literature, various THz receivers capable of detecting the incoming signal exist [40–42], verifying the feasibility of

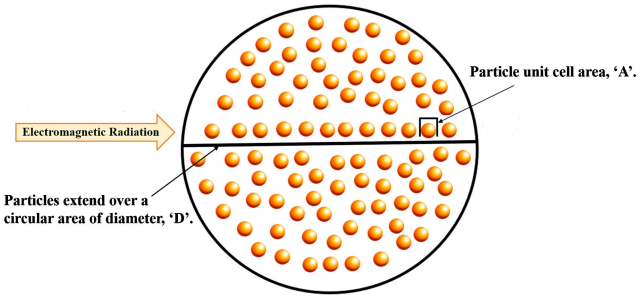


**Fig. 2** *System of an ensemble of identical particles extending over a circular area of diameter, D, with a unit cell area, A*

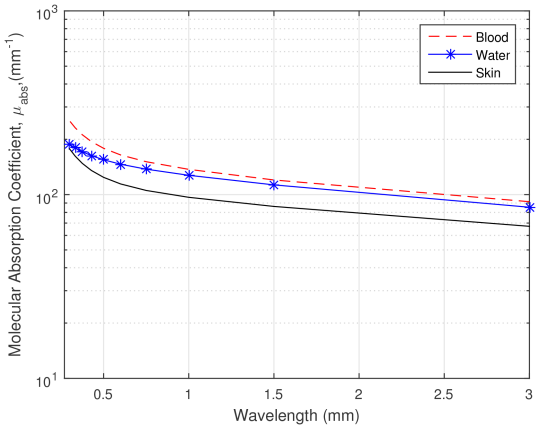


**Fig. 3** *Molecular absorption coefficient, $\mu_{abs}$, for different human tissues versus wavelength at THz ($\lambda = 300\,\mu$m to 3 mm)*

**Table 2** Radii of various body particles [34]

| body components | radius, m |
|---|---|
| water particle | $1.4 \times 10^{-10}$ |
| skin cell | $30 \times 10^{-6}$ |
| red blood cell | $4 \times 10^{-6}$ |

intrabody communication in the THz band. It is to be noted that both the THz transmitters as well as receivers have been selected based on both power and size constraints presenting a suitable platform for further implementation in intrabody scenarios, especially for the devices utilising graphene. In the case of transmitters, on-chip antennas, which are known for occupying small areas, are used. Likewise, in terms of receivers, transistors are deployed ensuring a low order of magnitude sizes. The authors in [43] present a detailed review of the most recent advancements in THz technologies.

For completeness, the previously presented link budget calculations have been repeated by taking into account the antenna gain value of 2.15 dBi, as it corresponds to a half-wavelength dipole antenna which models the expected performance of a nanoantenna deployed in an intrabody communication scenario. Hence, a total gain of 4.3 dBi has been added based on (41) corresponding to the antenna transmit and receive gains, respectively. The results are illustrated in Table 4. It can be stemmed that even by taking into account the antenna gain, the THz technologies are still capable of capturing the propagating signal through the body.

### *4.5 Photo-thermal effect*

The photo-thermal intrabody temperature effect is computed for blood in order to illustrate its influence on the various constituents such as blood plasma and on different types of particles including platelets, red blood cells, and white blood cells. Hence, the electrical and thermal properties of blood summarised in Table 5 have been used. It must be pointed out that the original heat source stems from fields created by a nanoantenna at a given distance.

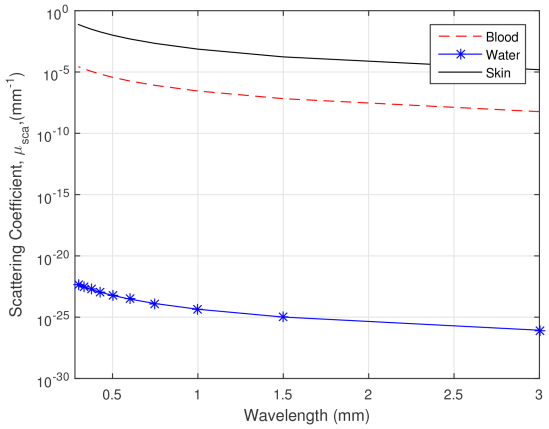


**Fig. 4** *Scattering coefficient, $\mu_{sca}$, for different human tissues versus wavelength at THz ($\lambda = 300\,\mu$m to 3 mm)*

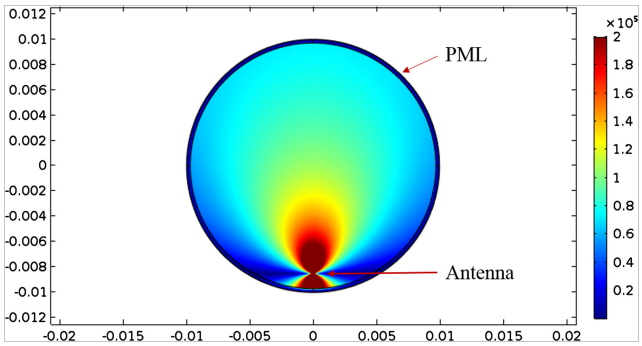


**Fig. 5** *Electric field intensity (V/m) of a circular cross section composed of a three-layer human tissue: COMSOL multiphysics simulation model*

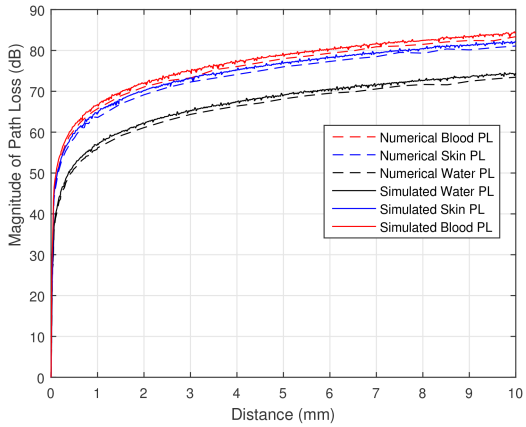


**Fig. 6** *Magnitude of total path loss factor, $L_{tot}$, at ($\lambda = 300\,\mu$m), when short range communication between (0.01–10 mm) is considered*

**Table 3** Link budget calculation

| Parameter | Value | Reference |
|---|---|---|
| frequency of operation | 1 THz | — |
| propagating distance | 1 mm | — |
| transmit power | 1 mW | [38, 39] |
| assumed SNR | 10 dB | — |
| path loss | 65.9 dB | Fig. 6 |

Fig. 7 provides the temperature increase experienced by multiple red blood cells. Such an accumulative effect arises from the addition of heat fluxes generated by the single particles. The more the particles, the stronger the temperature increases that appear in the system. It is evident that for smaller inter-particle distances, the interaction between the temperature fields is stronger; the reason behind this is that the time needed for thermal fields from neighbouring particles to overlap is shorter for smaller

**Table 4** Gain effect on link budget calculation

| range of operation | $P_R$, W | receiver sensitivity |
|---|---|---|
| THz band | 708 pW | 70.8 pW |

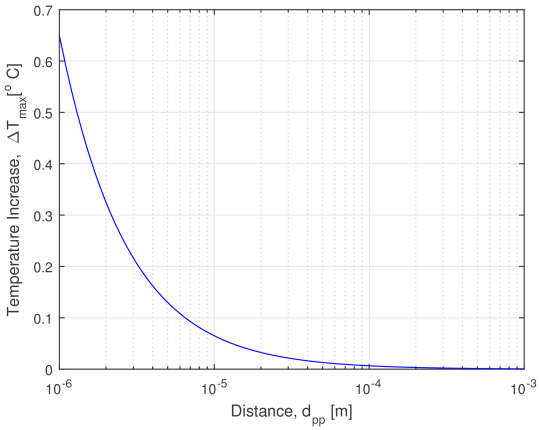


**Fig. 7** *Temperature increase due to the collective heating of 1000 red blood cells at* 300 $\mu$m

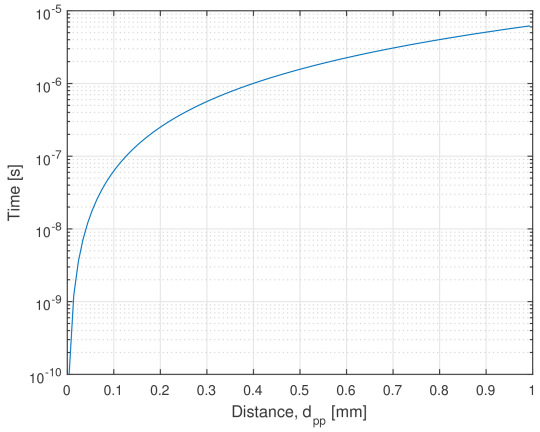


**Fig. 8** *Time scale for heat diffusion of a single particle*

particle–particle separation. In Fig. 8, we plot the heating time versus the particle–particle separation. It is evident that as this separation increases, the heating time required also increases. This observation verifies the decaying temperature curve attained in Fig. 7.

The results of such observations are further verified by utilising the COMSOL model provided in Fig. 9. In fact, one of the critical features that distinguish this software is its bio-heat interface which is considered a perfect tool for simulating thermal effects in human tissues and other biological systems. The model provided consists of a red blood cell suspended in a liquid medium. The thermal parameters used in COMSOL are analogues to those used in Matlab and presented in Table 5. Both electromagnetic and time-dependent bio-heat studies were applied to the constructed model, having a wavelength of 300 $\mu$m. A point dipole has been used as the heating source.

The temperature discrepancies throughout a cell exposed to a heating duration of 10 ms is presented in Fig. 10. It is perceived that the cell starts to heat up from the side the antenna radiates through it, and then the cell itself turns into a heat source and dissipates the heat to the medium. This finding is verified by noting that the temperature variation at the cell centre is the highest in comparison with the cell membrane and to that between the cell and the antenna.

Although the pulse duration utilised in Fig. 10 is 10 ms, still the temperature increase is only 1.7°C which alleviates the concerns associated with THz intrabody applications. In addition, such a result opens the door towards the THz signal requirements in terms of duration and strength. The heating time may be further increased

**Table 5** Simulation parameters [44, 45, 46]

| Parameter | Symbol | Value | Unit |
|---|---|---|---|
| red blood cell thermal conductivity | $\kappa_p$ | 0.52 | W/m/°C |
| red blood density | $\rho$ | 1025 | kg/m$^3$ |
| red blood cell specific heat capacity | $C_p$ | 3617 | J/kg/°C |
| blood plasma thermal conductivity | $\kappa_0$ | 0.58 | W/m/°C |
| light intensity | $I_0$ | $10^4$ | W/cm$^2$ |

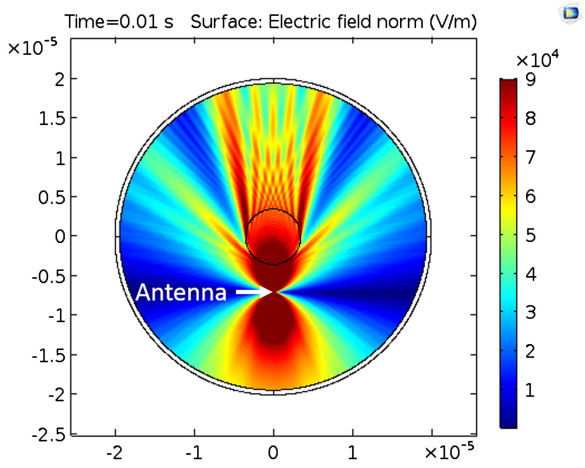


**Fig. 9** *Single red blood cell exposed to an electromagnetic wave with the duration of 10 ms and a dipole moment of 1 mA·m*

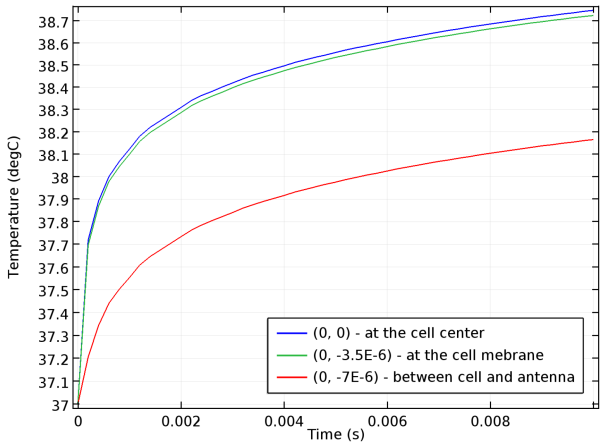


**Fig. 10** *Temperature variation as a function of time experienced at the cell centre, at the cell membrane and between the cell and the antenna for a heating time of 10 ms and a dipole moment of 1 mA·m at* 300 $\mu$m

and used for therapeutic applications including hyperthermia, which is utilised for localised cancer treatment without impacting the surrounding normal tissues [47]. In particular, by further increasing the signal strength of the point dipole, elevation in the temperature is witnessed as indicated in Fig. 11.

## 5 Conclusion

This study developed a channel model for predicting the effect of THz electromagnetic propagation through a homogeneous intrabody system. The presented model is novel since it takes into account the combined effect of three main propagation phenomena encountered in intrabody communication including spreading, molecular absorption, and scattering. The spreading effect has been accurately quantified by incorporating the directivity of the nanoantenna. Investigation of molecular absorption demonstrated that blood molecules are more absorbent in comparison with other body composites. Moreover, scattering has been accurately computed by taking into account the size of the scatterer nanoparticles with respect to the wavelength in the THz band. The combined effects of the three main propagation phenomena in

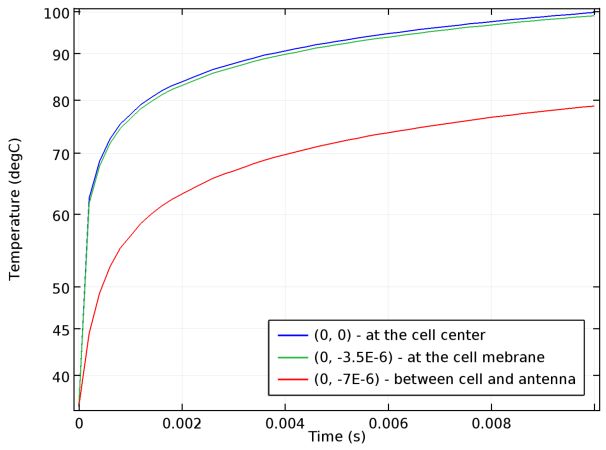


**Fig. 11** *Temperature variation as a function of time experienced at the cell centre, at the cell membrane and between the cell and the antenna for a heating time of 10 ms and a dipole moment of 6 mA·m at* 300 $\mu$m

intrabody communication facilitate the design and deployment of iWNSNs. It must be highlighted that due to the recent advancements in THz technologies, novel THz transmitters and receivers have been developed facilitating the communication between nanodevices and opening the door to potentially biocompatible applications of iWNSNs. Furthermore, a photo-thermal model that captures the effect of molecular absorption from electromagnetic fields is presented. This diffusive heat flow phenomenon results in temperature changes which ought to be quantised in order to understand its implications. Numerical results obtained show that both the signal pulse duration and the dipole moments of the THz signal are important controlling parameters required for initiating practical communication strategies for efficient intrabody communication as well as alleviating any concerns associated with deploying THz frequencies.

## 6 References


[1] Akyildiz, I.F., Jornet, J.M., Pierobon, M.: 'Nanonetworks: a new frontier in communications', *Commun. ACM*, 2011, **54**, (11), pp. 84–89

[2] Shubair, R.M., Elayan, H.: 'In vivo wireless body communications: state-of-the-art and future directions'. IEEE 2015 Loughborough Antennas & Propagation Conf. (LAPC), Loughborough, 2015, pp. 1–5

[3] Akyildiz, I.F., Fekri, F., Sivakumar, R., *et al.*: 'Monaco: fundamentals of molecular nano-communication networks', *IEEE Wirel. Commun.*, 2012, **19**, (5), pp. 12–18

[4] Santagati, G.E., Melodia, T., Galluccio, L., *et al.*: 'Ultrasonic networking for e-health applications', *IEEE Wirel. Commun.*, 2013, **20**, (4), pp. 74–81

[5] Jornet, J.M., Akyildiz, I.F.: 'Graphene-based plasmonic nano-antenna for terahertz band communication in nanonetworks', *IEEE J. Sel. Areas Commun.*, 2013, **31**, (12), pp. 685–694

[6] Elayan, H., Shubair, R.M., Alomainy, A., *et al.*: 'In-vivo terahertz EM channel characterization for nano-communications in WBANS'. 2016 IEEE Int. Symp. on Antennas and Propagation (APSURSI), June 2016, pp. 979–980

[7] Nafari, M., Jornet, J.M.: 'Metallic plasmonic nano-antenna for wireless optical communication in intra-body nanonetworks'. Proc. 10th EAI Int. Conf. on Body Area Networks, ICST (Institute for Computer Sciences, Social-Informatics and Telecommunications Engineering), 2015, pp. 287–293

[8] Biagioni, P., Huang, J.-S., Hecht, B.: 'Nanoantennas for visible and infrared radiation', *Rep. Prog. Phys.*, 2012, **75**, (2), p. 024402

[9] Elayan, H., Shubair, R.M., Jornet, J.M.: 'Bio-electromagnetic thz propagation modeling for in-vivo wireless nanosensor networks', 2017 11th European Conf. on Antennas and Propagation (EUCAP), March 2017, pp. 426–430

[10] Vander Vorst, A., Rosen, A., Kotsuka, Y.: '*RF/microwave interaction with biological tissues*', vol. 181 (John Wiley & Sons, Hoboken, New Jersey, 2006)

[11] Balanis, C.A.: '*Antenna theory: analysis and design*' (John Wiley & Sons, Hoboken, New Jersey, 2016)

[12] Lin, H., Fumeaux, C., Fischer, B.M., *et al.*: 'Modelling of sub-wavelength THz sources as Gaussian apertures', *Opt. Express*, 2010, **18**, (17), pp. 17 672–17 683

[13] Calloway, D.: 'Beer–Lambert law', *J. Chem. Educ.*, 1997, **74**, (7), p. 744

[14] Jornet, J.M., Akyildiz, I.F.: 'Channel modeling and capacity analysis for electromagnetic wireless nanonetworks in the terahertz band', *IEEE Trans. Wirel. Commun.*, 2011, **10**, (10), pp. 3211–3221

[15] Martelli, F.: '*Light propagation through biological tissue and other diffusive media: theory, solutions, and software*' (SPIE Press, 2010). Available at https://books.google.com/books?id=5pEDQgAACAAJ

[16] Yaws, K., Mixon, D., Roach, W.: 'Electromagnetic properties of tissue in the optical region', Biomedical Optics (BiOS) 2007, International Society for Optics and Photonics, 2007, pp. 643 507–643 507

[17] Xu, J., Plaxco, K.W., Allen, S.J.: 'Probing the collective vibrational dynamics of a protein in liquid water by terahertz absorption spectroscopy', *Protein Sci.*, 2006, **15**, (5), pp. 1175–1181

[18] Kindt, J., Schmuttenmaer, C.: 'Far-infrared dielectric properties of polar liquids probed by femtosecond terahertz pulse spectroscopy', *J. Phys. Chem.*, 1996, **100**, (24), pp. 10 373–10 379

[19] Reid, C.B., Reese, G., Gibson, A.P., *et al.*: 'Terahertz time-domain spectroscopy of human blood', *IEEE J. Biomed. Health Inform.*, 2013, **17**, (4), pp. 774–778

[20] Chu, B.: '*Laser light scattering*' (Elsevier, 1974)

[21] Calvert, J.G.: 'Glossary of atmospheric chemistry terms (recommendations 1990)', *Pure Appl. Chem.*, 1990, **62**, (11), pp. 2167–2219

[22] Fozard, J.A.: 'Diffraction and scattering of high frequency waves'. Ph.D. dissertation, University of Oxford, 2005

[23] Friedlander, S.: '*Smoke, dust, and haze: fundamentals of Aerosol dynamics (topics in chemical engineering)*' (Oxford University Press, Oxford, 2000), Available at https://books.google.com/books?id=fNIeNvd3Ch0C

[24] Bohren, C.F., Huffman, D.R.: '*Absorption and scattering of light by small particles*' (John Wiley & Sons, Hoboken, New Jersey, 2008)

[25] Bates, D.: 'Rayleigh scattering by air', *Planet. Space Sci.*, **32**, (6), pp. 785–790, 1984

[26] Hulst, H.C., van de Hulst, H.C.: '*Light scattering by small particles*' (Courier Corporation, New York, 1957)

[27] Kokhanovsky, A.A.: '*Light scattering media optics*' (Springer Science & Business Media, New York, 2004)

[28] Piro, G., Yang, K., Boggia, G., *et al.*: 'Terahertz communications in human tissues at the nanoscale for healthcare applications', *IEEE Trans. Nanotechnol.*, 2015, **14**, (3), pp. 404–406

[29] Zhang, R., Yang, K., Alomainy, A., *et al.*: 'Modelling of the terahertz communication channel for in-vivo nano-networks in the presence of noise'. 2016 16th Mediterranean Microwave Symp. (MMS), November 2016, pp. 1–4

[30] Donner, J.S., *et al.*: 'Thermo-plasmonics: controlling and probing temperature on the nanometer scale', 2014

[31] Baffou, G., Berto, P., Bermúdez Ureña, E., *et al.*: 'Photoinduced heating of nanoparticle arrays', *ACS Nano*, 2013, **7**, (8), pp. 6478–6488

[32] Govorov, A.O., Zhang, W., Skeini, T., *et al.*: 'Gold nanoparticle ensembles as heaters and actuators: melting and collective plasmon resonances', *Nanoscale Res. Lett.*, 2006, **1**, (1), pp. 84–90

[33] O'Neil, D.: '*Blood components*' (Palomar College, San Marcos, 2012)

[34] Erickson, H.P.: 'Size and shape of protein molecules at the nanometer level determined by sedimentation, gel filtration, and electron microscopy', *Biol. Proced. Online*, 2009, **11**, (1), p. 32

[35] Griffin, J.D., Durgin, G.D., Haldi, A., *et al.*: 'Rf tag antenna performance on various materials using radio link budgets', *IEEE Antennas Wirel. Propag. Lett.*, 2006, **5**, (1), pp. 247–250

[36] Griffin, J.D., Durgin, G.D.: 'Complete link budgets for backscatter-radio and RFID systems', *IEEE Antennas Propag. Mag.*, 2009, **51**, (2), pp. 11–25

[37] Schneider, T., Wiatrek, A., Preussler, S., *et al.*: 'Link budget analysis for terahertz fixed wireless links', *IEEE Trans. Terahertz Sci. Technol.*, 2012, **2**, (2), pp. 250–256

[38] Gu, Q.J., Xu, Z., Jian, H.-Y., *et al.*: 'Cmos thz generator with frequency selective negative resistance tank', *IEEE Trans. Terahertz Sci. Technol.*, 2012, **2**, (2), pp. 193–202

[39] Hillger, P., Grzyb, J., Lachner, R., *et al.*: 'An antenna-coupled 0.49 THz SiGe HBT source for active illumination in terahertz imaging applications'. 10th European Microwave Integrated Circuits Conf. (EuMIC), 2015, pp. 180–183

[40] Knap, W., Dyakonov, M., Coquillat, D., *et al.*: 'Field effect transistors for terahertz detection: physics and first imaging applications', *J. Infrared Millim. Terahertz Waves*, 2009, **30**, (12), pp. 1319–1337

[41] Kachorovskii, V.Y., Rumyantsev, S., Knap, W., *et al.*: 'Performance limits for field effect transistors as terahertz detectors', *Appl. Phys. Lett.*, 2013, **102**, (22), p. 223505

[42] Cai, X., Sushkov, A.B., Suess, R.J., *et al.*: 'Sensitive room-temperature terahertz detection via the photothermoelectric effect in graphene', *Nat. Nanotechnol.*, 2014, **9**, (10), pp. 814–819

[43] Elayan, H., Shubair, R.M., Jornet, J.M., *et al.*: 'Terahertz channel model and link budget analysis for intrabody nanoscale communication', *IEEE Trans. Nanobiosci.*, 2017, **16**, (6), pp. 491–503

[44] PA, H., Gennaro, D., Baumgartner, C., *et al.*: (2015, September) IT'IS database for thermal and electromagnetic parameters of biological tissues, version 3.0. Available at https://www.itis.ethz.ch/virtual-population/tissue-properties/overview/

[45] Fedele, D., Fusi, F.: 'Thermal effects of NIR laser radiation in biological tissue: a brief survey', *Energy Health*, 2010, **6**, pp. 10–15

[46] Liu, X., Lei, D.Y.: 'Simultaneous excitation and emission enhancements in upconversion luminescence using plasmonic double-resonant gold nanorods', *Sci. Rep.*, 2015, **5**, p. 15235

[47] Wust, P., Hildebrandt, B., Sreenivasa, G., *et al.*: 'Hyperthermia in combined treatment of cancer', *Lancet Oncol.*, 2002, **3**, (8), pp. 487–497